Stem Cell Research & Therapy

RESEARCH

Open Access

# Obesity modulates hematopoietic stem cell fate decision via IL-1β induced p38/MAPK signaling pathway

Jinxiao Yan[1,2,3†], Pan Zhang[1,2,4†], Xiru Liu[1,2,3], Chengwei Pan[5], Guolin Shi[1,2,3], Penghui Ye[1,2,3], Xiaohang Zou[1,2,3], Xiang Li[1,2,3], Xinmin Zheng[1,2,3], Yu Liu[6*] and Hui Yang[1,2,3*]

## Abstract

**Background** Obesity is accompanied by inflammation, which significantly affects the homeostasis of the immune microenvironment. Hematopoietic stem cells (HSCs), residing primarily in the bone marrow, play a vital role in maintaining and producing diverse mature blood cell lineages for the adult hematopoietic and immune systems. However, how HSCs development is affected by obese-promoting inflammation, and the mechanism by which HSC hematopoietic potency is affected by inflammatory signals originating from the obese-promoting changes on bone marrow niche remain unclear. This study elucidates the relationship between obesity-promoting inflammation and HSC fate determination.

**Methods** The obesity mice model was established by feeding C57BL/6J mice a high-fat diet (HFD) containing 60% kcal fat. After 6 weeks, HSCs were analyzed using flow cytometry and identified key inflammation cytokine. Transcriptome sequencing techniques were used to discern the distinct pathways in HSCs. Ultimately, confirming the biological mechanism of obesity-induced HSC fate changes via Anakinra blocking specific inflammatory signals.

**Results** Obesity caused by HFD changed the physical and biochemical properties of the bone marrow niche. In the HFD mice, the population of long-term HSCs in the bone marrow was decreased and facilitated HSCs differentiation towards the myeloid lineage. In addition, HFD increased expression of the inflammatory factor IL-1β in the bone marrow, and a significantly increased expression of *IL-1r1* and active p38/MAPK signaling pathway were detected in the HSCs. Inhibition of IL-1β further normalized the expression of genes in p38/MAPK pathway and reversed HSC fate.

**Conclusions** These findings have been demonstrated that the p38/MAPK signaling pathway in HSCs is activated by elevated levels of IL-1β within the HSC niche in obese models, thereby regulating HSC differentiation. It suggested a direct link between obesity-promoting inflammation and myeloid differentiation bias of HSCs in the HFD mice.

**Keywords** Obesity, Inflammation, Hematopoietic stem cells, Bone marrow niche, IL-1β

†Jinxiao Yan and Pan Zhang have contributed equally to this work.

*Correspondence:
Yu Liu
lycqx@aliyun.com
Hui Yang
kittyyh@nwpu.edu.cn
Full list of author information is available at the end of the article

**Graphical abstract**

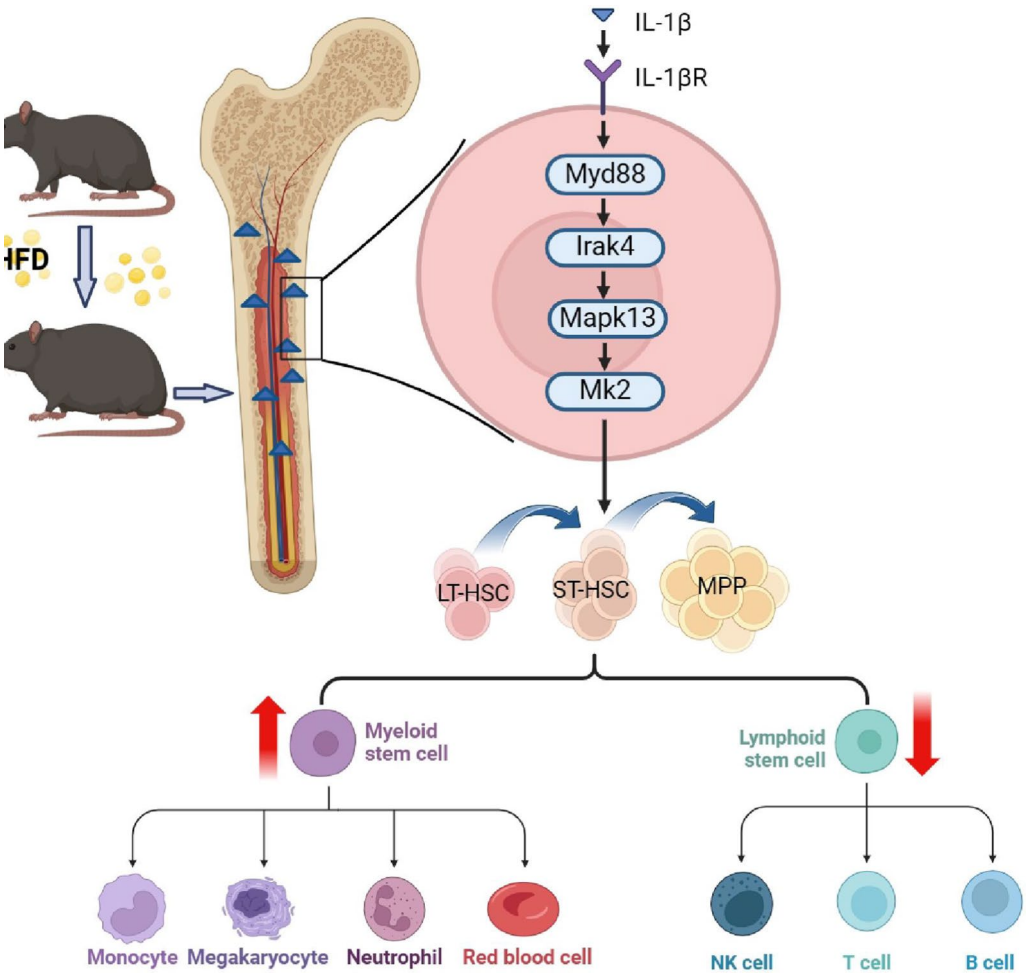


## Background

Obesity has emerged as a global epidemic over the past 5 decades [1], leading to various physiological issues and contributing significantly to conditions such as insulin resistance, atherosclerosis, hyperlipidemia, cancer, non-alcoholic fatty liver disease, among others [2]. Further exploration has increasingly revealed that inflammation plays a crucial role in the progression of obesity and its related complications [3]. Obesity elevates levels of inflammatory cytokines, including tumor necrosis factor-α (TNF-α), interleukin-6 (IL-6) and interleukin-1β (IL-1β), which cause chronic low-grade inflammation and lead to obesity-associated immune dysregulation in multiple organ systems [4]. Furthermore, obesity-promoting inflammation is characterized by the infiltration of immune cells into metabolic tissues, such as adipose tissue [5]. For instance, in comparison to mice fed a normal diet (ND), those fed a high-fat diet (HFD) exhibit increased macrophages in adipose tissue, which further promote the expression of inflammatory cytokines [6]. Additionally, the number of mast cells and natural killer T cells in the adipose tissue of obese animals increases, which in turn contribute to inflammation and metabolic disorders [4].

Bone marrow, an important immune organ, which is composed of various types of immune and blood cells. It has been reported that 8–20% of mononuclear cells in bone marrow belong to lymphocytes [7]. The homeostasis of bone marrow immune microenvironment is affected by age, metabolism and inflammation, and responds to infection and stress. Previous studies in rodent models induced by HFD have demonstrated elevated levels of pro-inflammatory cytokines (such as IL-1β, IL-6, and TNF-α) in bone marrow [8, 9]. Bone

marrow hematopoietic stem cells (HSCs) play a pivotal role in continuously replenishing the blood with millions of cells, including erythrocytes, T-cells, and B-cells [10–12]. The bone marrow provides the necessary mechanical support [13] and biochemical signals to maintain HSC characteristics, such as self-renewal and differentiation, which is essential for the maintaining hematopoietic homeostasis [11, 14, 15]. Substantial evidence now indicates that HSCs isolated from obese individuals display a tendency towards myeloid differentiation [7, 8, 16, 17]. However, it remains poorly understood whether specific inflammatory cytokines influence HSC fate transition in the bone marrow niche during the progression of obesity.

To investigate the impact of obesity-promoting bone marrow inflammation on HSC behaviors that determine changes in hematopoietic homeostasis, we constructed obesity mice model and analyzed the differences in the proliferation and differentiation of HSCs between obese and normal mice. Through comprehensive analysis of inflammatory cytokines in the bone marrow, IL-1β with higher expression emerged as a potent regulator of HSC fate changes in the obesity-associated bone marrow. Moreover, high-throughput transcriptome sequencing analysis of bone marrow HSCs revealed that IL-1β influences HSC fate by activating the p38/MAPK signaling pathway based on the ligand-receptor interaction.

We comprehensively report changes in proliferation and differentiation of HSCs, and clearly identify IL-1β induced by obesity plays a pivotal role that driving changes in the bone marrow HSCs. Our finding provides insights into better understanding of the influence of obesity on hemopoietic homeostasis, highlighting inflammation as a key mechanism regulating HSC differentiation. The IL-1β-triggered p38/MAPK signaling pathway offers a fresh look at how obesity impacts the decisions made by HSCs about their fate, revealing new insights into this process.

## Methods

### Experimental animals

The experimental subjects consisted of C57BL/6J male mice, adhering to the specific pathogen-free (SPF) standard. These mice, aged 5 weeks and weighing between 17 and 19 g, were procured from the Animal Culture Center of the Medical Research Institute at Xi'an Jiaotong University. Subsequently, they were housed within the animal facility at the Life College of Northwest Polytechnical University. To ensure acclimation, a one-week period of adaptive feeding was provided before the mice were randomly allocated into two groups. The experimental protocols involving mice followed the ARRIVE guidelines 2.0 (Animal Research: Reporting of In Vivo Experiments). These groups were administered distinct diets every three days: a 60% high-fat diet (Catalog No. D12492, Research Diets) and a 10% low-fat diet (Catalog No. D12450J, Research Diets) [17]. Weekly monitoring of mice weights was conducted throughout the study. To interrupt IL-1β signaling, a human IL-1β receptor antagonist, anakinra (SOBI, #AB666-5823407), was intraperitoneally injected at a dosage of 10mg/kg following four weeks of the HFD [18]. The mice were euthanized via cervical dislocation, preceded by anesthesia induced through inhalation of an overdose of isoflurane (Iflurane, CAS: 26675-46-7). It is important to note that in this study, no anesthesia of any kind was administered to the animals except during the euthanasia process. This specific procedure was designed with the aim of minimizing discomfort and pain experienced by the animals. A more detailed description of the anesthesia protocol utilized during euthanasia is provided in the subsequent section outlining the specific experimental methods.

### Sample preparation

The mouse was placed beneath a clean beaker, alongside a cotton ball pre-saturated with 100 μL of isoflurane. It was then allowed to remain undisturbed for a period of 1–2 min, during which time the mouse's tail could be gently pinched to assess its level of anesthesia. The experiment was commenced only after confirming that the mouse had achieved complete anesthesia and loss of consciousness, in order to minimize any potential pain or discomfort. Subsequently, blood was collected via ocular puncture. Following the completion of the blood collection procedure, the mouse was euthanized by cervical dislocation, and then the dissection experiment was conducted. Blood samples were collected from the orbital sinus and promptly pipetted into anticoagulant tubes for blood component analysis. The remaining blood was reserved for serum isolation [19]. After orbital blood collection, various adipose tissues were meticulously dissected, including epididymal fat, perirenal fat, subcutaneous fat, intestinal membrane fat, and dorsal brown fat, each of which was weighed using an electronic balance. Subsequently, femur and tibia specimens from the mice were immersed in 4% paraformaldehyde (Servicebio, #G1101-500ML) for a minimum of 48 h and then subjected to EDTA decalcification (Servicebio, #G1105-500ML) for approximately 15 days. The decalcification solution was replenished every three days, and the decalcification process was deemed successful when bone penetration occurred effortlessly. These specimens were then utilized for subsequent immunohistochemistry and hematoxylin and eosin (HE) staining. Following femur isolation, bone marrow was gently flushed out using PBS and

promptly frozen for sectioning. Atomic force microscopy was employed to determine the Young's modulus of fresh bone marrow tissue [20].

#### In vivo assays

Mice, following an overnight fast, received glucose solution (kermel, CAS: 50-99-7) via gavage at a dose of 1 g/kg. Blood glucose levels were monitored and recorded at 15-min intervals for up to 120 min post-gavage. Blood samples are obtained by pricking the tail of the mouse, and only 5 μl of blood need to be gently squeezed out each time. To reduce stress on the mouse, its tail can be gently stroked every day for a week before the experiment begins. This data was employed to construct blood glucose value curves at six time points, and the area under the curve was calculated to assess mouse blood glucose tolerance [21].

For the measurement of total cholesterol, triglyceride, low-density lipoprotein, and high-density lipoprotein levels in the serum, we used the corresponding kits (Nanjing Jiancheng, #A111-1-1, #A110-1-1, #A113-1-1, #A112-1-1) to conduct the tests.

#### Cell preparation and flow cytometry

Femoral and tibial specimens were collected after euthanizing the mice using the previously described methods. Bone marrow cells were harvested by flushing femurs and tibias and subsequently suspended in phosphate-buffered saline (PBS) containing 2% fetal bovine serum (FBS). After filtration to remove cell debris, red blood cells were lysed using red blood cell lysis buffer (TIANGEN, RT122-02) [19]. Bone marrow mononuclear cells were collected following two PBS washes.

HSCs were identified using phycoerythrin FITC-conjugated antibodies [22] against CD3, B220, CD11b, Ter-119, and Gr-1 (eBioscience, #22-7770-72); PE anti-Sca-1, clone D7 (eBioscience, #12-5981-81); AF700 anti-c-kit clone 2B8 (BioLegend, #105846); APC anti-CD34, clone MEC14.7 (BioLegend, #119309); BV510 anti-CD16/32, clone 93 (BioLegend, #101333); Pecp/cyanine 5.5 anti-IL-7R, clone A7R34 (BioLegend, #135022); BV421 anti-CD135, clone A2F10 (BioLegend, #135313). Flow cytometry (model: BDFACSCelesta, BD, San Jose, CA, USA) was employed for cell analysis, with data evaluation conducted using FlowJo (version 10.6.2) [19]. The Annexin V/PI apoptosis Kit (dojindo, #AD10) was utilized to assess bone marrow mononuclear cell apoptosis. Cell cycle analysis was performed using the PI/RNase Staining Kit (dojindo, #C543). Flow cytometry (model: BD FACS Celesta, BD, San Jose, CA, USA) was employed for analysis, and results were evaluated using FlowJo (version 10.6.2) [19, 23].

#### Colony formation assay

To compare the multi-lineage potential of HSCs form different groups, following isolation of bone marrow mononuclear cells, after accurate cell counting, 500–2000 cells were suspended in IMDM medium and 2% FBS to reach a volume of 0.1 mL. Subsequently, 1mL of Metho Cult® (M3434, stem cell technology, Canada) was added to each cell suspension to create a methylcellulose medium. The cell-methylcellulose mixture was vortexed vigorously and left undisturbed for approximately 5 min to allow bubbles to dissipate. Each 35 mm Petri dish was then inoculated with the cell-methylcellulose mixture, with two 35 mm Petri dishes placed in each 100 mm Petri dish. An additional 35 mm Petri dish containing 3 mL of sterile water was also included. The inoculated Petri dishes were incubated at 37 °C in a 5% $CO_2$ incubator for 12–14 days, with no disturbances during this period. Afterward, cell colonies became visible to the naked eye. Colonies were assessed, classified, and quantified using an inverted microscope [24].

#### $Lin^-$ $c\text{-}kit^+$ cells enrichment

A buffer comprising 5% serum was introduced into MACS [24, 25], and the resulting mixture was centrifuged at 300×g for 10 min to eliminate supernatant. Cells were resuspended in 40 μL of buffer after supernatant removal. Subsequently, 10 μL of biotin antibody cocktail was added and mixed thoroughly, followed by a 10 min incubation at 4 °C in darkness. After incubation, 30 μL of buffer was introduced, mixed, and then supplemented with 20 μL of anti-biotin microbeads. A 15 min incubation in darkness at 4 °C followed. Cells were then washed with 1000 μL of buffer, centrifuged at 300×g for 10 min to eliminate supernatant, and resuspended in 500μL of buffer. Magnetic separation using MS sorting columns was carried out. $Lin^-$ cells, which were not magnetically labeled, were collected. In the subsequent step, $Lin^-$ cells were collected and centrifuged at 300×g for 10 min to remove supernatant. Cells were resuspended in 80 μL of buffer, and 20 μL of CD117 magnetic beads were added. After thorough mixing, the cells were incubated at 4 °C for 15 min. Following incubation, cells were washed with 1000 μL of buffer, centrifuged at 300×g for 10 min to remove supernatant, and then resuspended in 500 μL of buffer. The sorting column was moistened with 500 μL of buffer, and the cell suspension was introduced into the column. Cells were collected from the sorting column after the cell drops ceased. Subsequently, the sorting column was washed with 500 μL of buffer three times. Upon removal from the sorter, the sorting column was placed on a 15 mL sterile centrifuge tube. Finally, 1000 μL of buffer was rapidly introduced to elute magnetically

labeled cells in the sorting column, yielding $Lin^-$ $c\text{-}kit^+$ cells, which was used for transcriptome sequencing.

### Transcriptome sequencing and data analysis

The transcriptome sequencing project was entrusted to Hangzhou Lianchuan Biotechnology Co., Ltd. The intricate RNA-Seq library construction process encompassed a series of meticulous steps: initially, total RNA extraction; subsequently, a rigorous quality assessment of the extracted RNA; followed by the purification of mRNA and its fragmentation; then, cDNA synthesis; further, PCR-mediated enrichment of library fragments; next, a thorough quality inspection of the constructed library; ultimately, sequencing on the advanced Illumina platform. The analysis of the acquired RNA-Seq data underwent a series of refined procedures: commencing with the retrieval of offline sequencing data, followed by data filtration to ensure purity; then, a comprehensive quality assessment; subsequent alignment to the reference genome; quantification of gene expression levels; differential expression analysis to identify significant changes; cluster analysis, including Pearson correlation and Principal Component Analysis (PCA), to uncover patterns and relationships; and lastly, enrichment analysis leveraging the Lianchuan Cloud platform, encompassing gene ontology (GO) and kyoto encyclopedia of genes and genomes (KEGG) pathways, to decipher the biological significance of the results. The transcriptome sequencing data are included in the supplementary materials.

### Quantitative real-time PCR

Total RNA was extracted from MNCs using TRIzol (Invitrogen, #10296010) and then reverse-transcribed using cDNA reverse transcription kit (TransGen, #AU341) following the manufacturer's protocol (50 °C for 5 min, 85 °C for5s). A qRT-PCR was conducted using SYBR-green SuperMix (TransGen, AQ601) on real-time PCR systems (Bio-Rad, CFX96). The cDNA was subjected to 40 PCR cycles (95 °C for 3 min, 95 °C for 10 s, 56 °C for 30 s, 72 °C for 30 s). mRNA expression levels were normalized to β-actin mRNA and quantified using the $2^{-\Delta\Delta Ct}$ method. Primer sequences are provided in Table 1 (primers designed by Shenggong, with primer specificity verified through agarose gel electrophoresis following qRT-PCR) [19].

### Statistical analysis

Data were presented as means ± standard error of the mean (SEM). Comparisons between two groups were evaluated using an unpaired Student's t-test, while comparisons involving more than two groups were analyzed via a one-way ANOVA, followed by Tukey's test (GraphPad Prism 9.0). The values of $^*P < 0.05$, $^{**}P < 0.01$, $^{***}P < 0.001$ and $^{****}P < 0.0001$ were considered to be statistically significant.

**Table 1** Primer sequence

| Target gene | Primer sequence |
|---|---|
| *β-actin* | Forward 5′-GCTGTATTCCCCTCCATCGTG-3′<br>Reverse 5′-CACGGTTGGCCTTAGGGTTCAG-3′ |
| *Il-1β* | Forward 5′-CACTACAGGCTCCGAGATGAACAA-3′<br>Reverse 5′-TGTCGTTGCTTGGTTCTCCTTGTAC-3′ |
| *Il-6* | Forward 5′-CACTGGTCTTTTGGAGTTTGAG-3′<br>Reverse 5′-GGACTTTTGTACTCATCTGCAC-3′ |
| *Tnf-α* | Forward 5′-ATGTCTCAGCCTCTTCTCATTC-3′<br>Reverse 5′-GCTTGTCACTCGAATTTTGAGA-3′ |
| *Il-10* | Forward 5′-GCTCTTACTGACTGGCATGAG-3′<br>Reverse 5′-CGCAGCTCTAGGAGCATGTG-3′ |
| *Il-12* | Forward 5′-TGGTTTGCCATCGTTTTGCTG-3′<br>Reverse 5′-ACAGGTGAGGTTCACTGTTTCT-3′ |
| *Ccna2* | Forward 5′-GCCTTCACCATTCATGTGGAT-3′<br>Reverse 5′-TTGCTGCGGGTAAAGAGACAG-3′ |
| *Cdk1* | Forward 5′-AGAAGGTACTTACGGTGTGGT-3′<br>Reverse 5′-GAGAGATTTCCCGAATTGCAGT-3′ |
| *Csfr1* | Forward 5′-TGTCATCGAGCCTAGTGGC-3′<br>Reverse 5′-CGGGAGATTCAGGGTCCAAG-3′ |
| *Gata1* | Forward 5′-GTCCTCACCATCAGATTCCACAG-3′<br>Reverse 5′-GAGTGCCGTCTTGCCATAGG-3′ |
| *Gfi-1* | Forward 5′-GCCTCAGATGACCAGGGGA-3′<br>Reverse 5′-TGTTTGGACCCTCGGATACTC-3′ |
| *Runx-1* | Forward 5′-TTTCAAGGTACTCCTGCCTGA-3′<br>Reverse 5′-CAGTGAGAAGGACCAGAGACT-3′ |
| *Stat3* | Forward 5′-CAATACCATTGACCTGCCGAT-3′<br>Reverse 5′-GAGCGACTCAAACTGCCCT-3′ |
| *Stat6* | Forward 5′-CTCTGTGGGGCCTAATTTCCA-3′<br>Reverse 5′-CATCTGAACCGACCAGGAACT-3′ |
| *Il-1r1* | Forward 5′-GTGCTACTGGGGCTCATTTGT-3′<br>Reverse 5′-GGAGTAAGAGGACACTTGCGAAT-3′ |
| *Myd88* | Forward 5′-TCATGTTCTCCATACCCTTGGT-3′<br>Reverse 5′-AAACTGCGAGTGGGGTCAG-3′ |
| *Irak4* | Forward 5′-CATACGCAACCTTAATGTGGGG-3′<br>Reverse 5′-GGAACTGATTGTATCTGTCGTCG-3′ |
| *Mapk13* | Forward 5′-ATGAGCCTCACTCGGAAAAGG-3′<br>Reverse 5′-GCATGTGCTTCAAGAGCAGAA-3′ |
| *MK2* | Forward 5′-TTCCCCCAGTTCCACGTCA-3′<br>Reverse 5′-GCAGCACCTTCCCGTTGAT-3′ |

## Results

### Establishment of obesity model

To systematically elucidate the impact of obesity on HSC proliferation and differentiation, we established an obesity mice model by subjecting C57BL/6J mice to a high-fat diet (HFD, containing 60 kcal% fat) and a normal diet (ND, containing 10 kcal% fat) [17]. After 6 weeks, the mice in the HFD group exhibited a 20% increase in body weight compared to those in the ND group (Fig. 1A, B). Body mass index (Fig. 1C) and Lee's index (Fig. 1D) was assessed, which demonstrated significant improvements

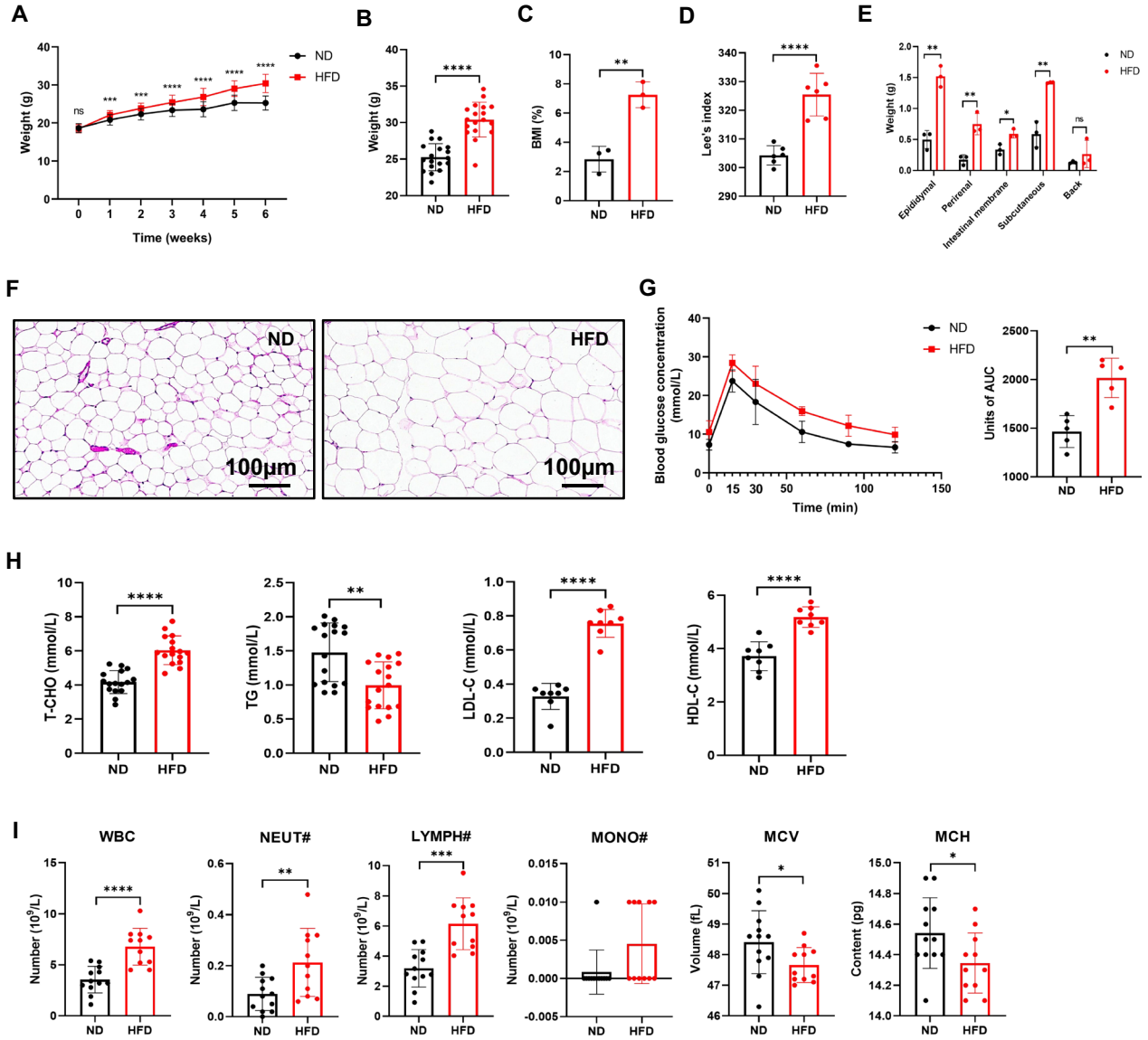


**Fig. 1** Establishment of obesity animal model. (**A**) The change of body weight with time; (**B**) Body; (**C**) BMI; (**D**) Lee's index; (**E**) Fat index; (**F**) Morphology of adipocytes; (**G**) The blood glucose value changes with time; Area under curve; (**H**) T-CHO, TG, LDL-C, HDL-C; (**I**) Peripheral blood components. (data = mean ± standard error, * represents a significant difference compared with ND group, *$p < 0.05$, **$p < 0.01$, ***$p < 0.001$, ****$p < 0.0001$, ns represents no significant difference between the two groups. body mass index (BMI); mean corpuscular volume (MCV); mean corpuscular hemoglobin content (MCH); white blood cells (WBC); neutrophils (NEUT); lymphocytes (LYMPH); monocytes (MONO); Total Cholesterol (T-CHO) Triglyceride (TC); High Density Lipoprotein (HDL-C); Low Density Lipoprotein (LDL-C))

in the HFD group. Furthermore, the HFD group mice exhibited a significant increase in the all areas of fat mass (Fig. 1E), accompanied by an expansion in adipocyte size (Fig. 1F). Obesity can lead to metabolic disturbances in mice [26]. Therefore, we investigated alterations in glucose and lipid metabolism in HFD mice. The results indicated that HFD significantly elevated blood glucose levels and reduced glucose tolerance in mice (Fig. 1G). In addition, the results of four serum lipid tests demonstrated increased blood lipid content in HFD mice (Fig. 1H). These findings collectively suggest that HFD disrupts metabolic homeostasis in mice. For the assessment of hematological parameters in mice, the analysis of blood components in both groups was conducted. Compared to the ND group, the HFD group exhibited reduced mean corpuscular volume and mean corpuscular hemoglobin content. Additionally, the HFD group mice showed a significant increase in the number of white blood cells, neutrophils, lymphocytes, and monocytes (Fig. 1I), indicating an inflammatory state induced by HFD. These data

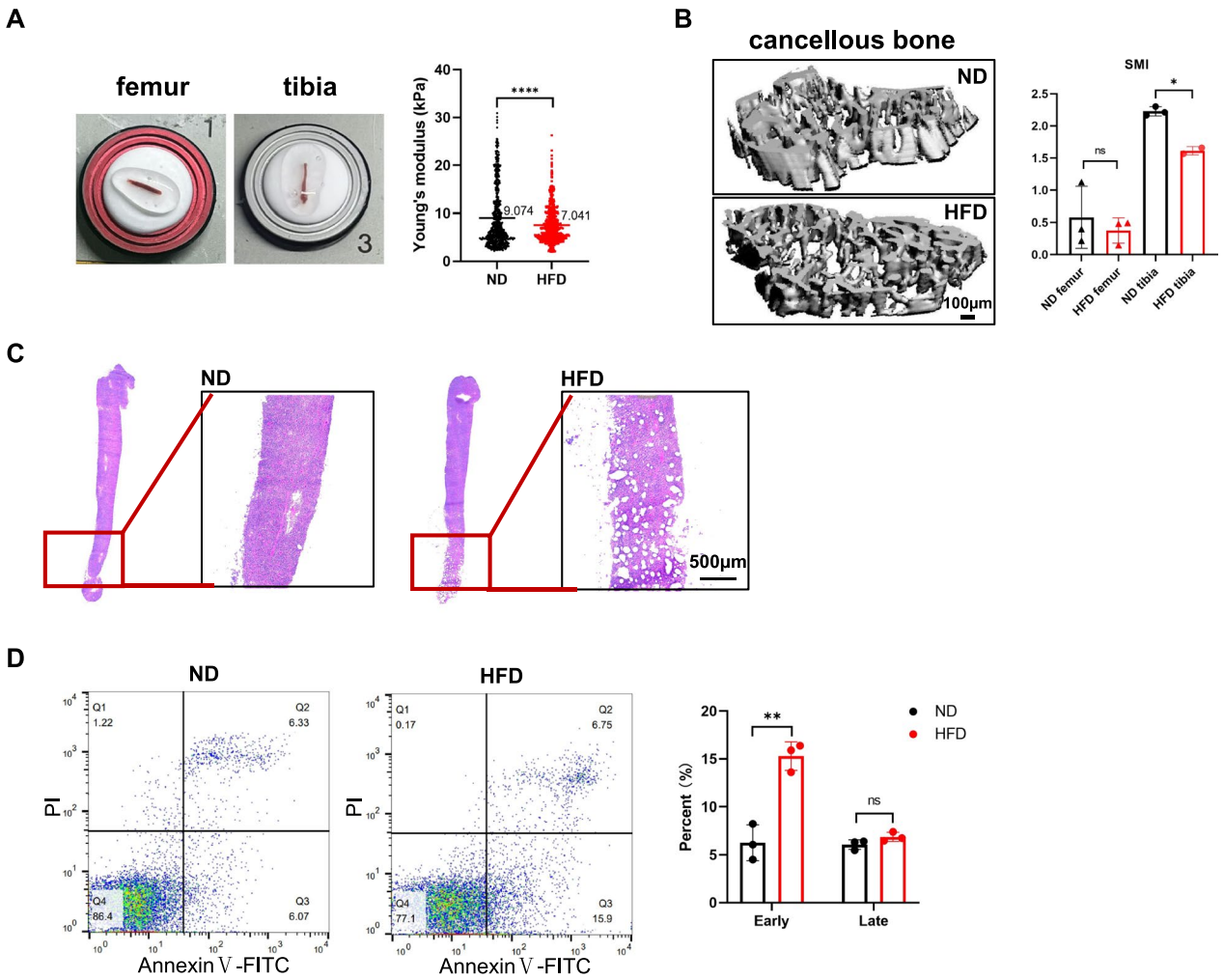


**Fig. 2** Deregulation of the bone architecture and BM niches by HFD exposure. (**A**) Stiffness measurement by Young's modulus in young (Data were obtained from 600 assays); (**B**) Micro-CT scan morphology and SMI value of mice bone structure; (**C**) HE staining morphology of bone marrow; (**D**) Statistics of apoptosis of bone marrow mononuclear cells. (data = mean ± standard error, *represents a significant difference compared with ND group, *$p < 0.05$, **$p < 0.01$, ***$p < 0.001$, ****$p < 0.0001$, ns represents no significant difference between the two groups. structural model index (SMI))

highlight the alteration of physiological parameters as well as the immune system in mice subjected to HFD for 6 weeks.

### Obesity causes the biomechanical changes in the bone marrow

For identify the underlying link between HSC fate decision with obesity, changes in the bone marrow, that primarily maintain HSC function were investigated. Atomic force microscopy (AFM) measurements were performed on freshly extracted bone marrow samples to assess the biomechanical properties of the HSC niche [20]. Despite the generally low stiffness of bone marrow, obesity resulted in a decrease in Young's modulus of bone marrow (Fig. 2A), indicating that the bone marrow becomes softer as obesity progresses. Micro-CT analysis was then performed to explore whether HFD induces alterations in bone structure. The result revealed a lower structural model index in HFD mice compared to ND mice, suggesting transformations in the trabecular bone structure (Fig. 2B). Additionally, hematoxylin and eosin staining showed obvious adipose cell infiltration within bone marrow tissue in the HFD mice (Fig. 2C). To assess cellular apoptosis, caspase levels within the bone marrow were measured, revealing an increase in caspase-positive cells in the context of obesity (Fig. 2D). These findings collectively highlight that obesity disrupts the mechanical properties and homeostasis of the bone marrow niche.

### HFD exposure leads to a reduction in the HSCs pool with active differentiation

In order to elucidate the influence of obesity on HSC fate, flow cytometry was used to analyze HSC proliferation and differentiation of obesity mice model. Assessment of the percentage of LSK ($Lin^-$ $Scal\text{-}1^+$ $c\text{-}kit^+$) cells in the bone marrow niche revealed a significant decrease in the HFD group compared to the ND group (Fig. 3A). Furthermore, quantification of HSC sub-populations, including long-term HSCs (LT-HSCs, $Lin^-$ $Scal\text{-}1^+$ $c\text{-}kit^+$ $CD34^-$ $CD135^-$), short-term HSCs (ST-HSCs, $Lin^-$ $Scal\text{-}1^+$ $c\text{-}kit^+$ $CD34^+$ $CD135^-$), and multipotent progenitors (MPPs, $Lin^-$ $Scal\text{-}1^+$ $c\text{-}kit^+$ $CD34^+$ $CD135^+$), indicated a decreased percentage of LT-HSCs and an increased percentage of MPPs in HFD mice bone marrow compared to that of ND mice (Fig. 3B). Additionally, we observed a reduced proportion of LSK cells in the G1 phase but an increased proportion in the S/G2/M phase in HFD mice (Fig. 3C). These findings indicate that HFD exposure induces alterations in HSC proliferation and cell cycle dynamics, leading to a reduction in the HSCs pool. Notably, the subset of these HSCs appears to transition from a quiescent state to an actively differentiating state.

To determine the change in HSC differentiation direction after HFD exposure, the percentages of common lymphoid progenitor (CLP, $Lin^-$ $CD135^+$ $IL\text{-}7R^+$), common myeloid progenitor (CMP, $Lin^-$ $c\text{-}kit^+$ $CD34^+$ $CD16/32^-$), megakaryocyte/erythrocyte progenitor (MEP, $Lin^-$ $c\text{-}kit^+$ $CD34^-$ $CD16/32^-$), and granulocyte/monocyte progenitor (GMP, $Lin^-$ $c\text{-}kit^+$ $CD34^+$ $CD16/32^+$) was quantified. Data revealed a shift towards increased CMP and GMP populations in the bone marrow of HFD mice, whereas CLP and MEP populations were diminished compared to ND mice (Fig. 3D). Consequently, HFD promoted the differentiation of HSCs toward myeloid lineages. Microscopic examination of mouse bone marrow cell colonies after 14 days of culture indicated an increase in granulocyte colony-forming unit and granulocyte–macrophage colony-forming unit in the HFD group (Fig. 3E). These observations collectively demonstrate that HFD exposure induces heightened division activity in HSCs and shifts their differentiation trajectory from lymphoid to myeloid lineages.

### Obesity-promoting IL-1β expression is a potential factor that triggers HSC fate changes

To gain a deeper understanding of the key inflammatory cytokines induced by HFD that influence HSC fate decision, the expression of inflammatory genes within the bone marrow niche was measured. Results revealed increased expression of *Il-1β*, *Il-6*, *Tnf-α*, *Il-10*, and *Il-12* genes in the HFD group compared to the ND group, with *Il-1β* exhibiting the most significant change (Fig. 4A). Previous findings indicated that HFD could shift the HSC state from quiescence to differentiation, in particular towards the myeloid lineage. Therefore, the expression levels of genes related to HSC behavior and differentiation were further determined. Figure 4B displays the expression of cell cycle activators *Cdk1* and *Ccna2*, active HSCs genes *Stat3* and *Stat6*, and HSC-related myeloid differentiation genes *Csfr1*, *Runx1*, *Gfi-1*, and *Gata-1*. To identify key inflammatory cytokines impacting HSC differentiation, the Pearson correlation between inflammatory genes and HSC functional genes was analyzed (Fig. 4C). Results indicated that *Il-1β* is the inflammatory gene most strongly associated with molecular changes of HSCs. To further ascertain whether obesity affects IL-1β levels within the HSCs niche, immunohistochemistry experiments were conducted, demonstrating an increase in IL-1β-positive areas in the bone marrow following a HFD regimen (Fig. 4D). In conclusion, it can be concluded that IL-1β induced by obesity plays a pivotal role as an inflammatory cytokine driving changes in the fate of bone marrow HSCs.

### IL-1β drives alterations in the differentiation potential of HSCs via activation of the p38/MAPK pathway

For unravel the mechanism behind HFD-induced myeloid differentiation of HSCs, LK ($Lin^-$/$c\text{-}kit^+$) cells from HFD and ND mice were sorted from mouse bone marrow to conduct a transcriptome analysis. Principal component analysis (PCA) distinctly separated the two groups (Fig. 5A). A total of 414 differentially expressed genes were identified, consisting of 373 up-regulated and 41 down-regulated genes in the HFD when compared to the ND (Fig. 5B). GO enrichment analysis revealed several enriched GO terms in HFD, including "inflammatory

(See figure on next page.)

**Fig. 3** Changes in proliferation and differentiation of HSCs after 6 weeks of HFD. (**A**) Statistics of the proportion of LSK cells in bone marrow mononuclear cells; (**B**) Proportion of LSK cell subsets; (**C**) Cell cycle of HSCs; (**D**) Lineage differentiation of hematopoietic stem progenitor cells; (**E**) The microscope morphology of different colony forming units. (data = mean ± standard error, * represents a significant difference compared with ND group, $*p < 0.05$, $**p < 0.01$, $***p < 0.001$, $****p < 0.0001$, ns represents no significant difference between the two groups. colony forming units (CFU); CFU-granulocyte–macrophage progenitor (CFU-GM); CFU-granulocyte, erythrocyte, monocyte and megakaryocyte (CFU-GEMM); Burst forming unit-erythroid (BFU-E))

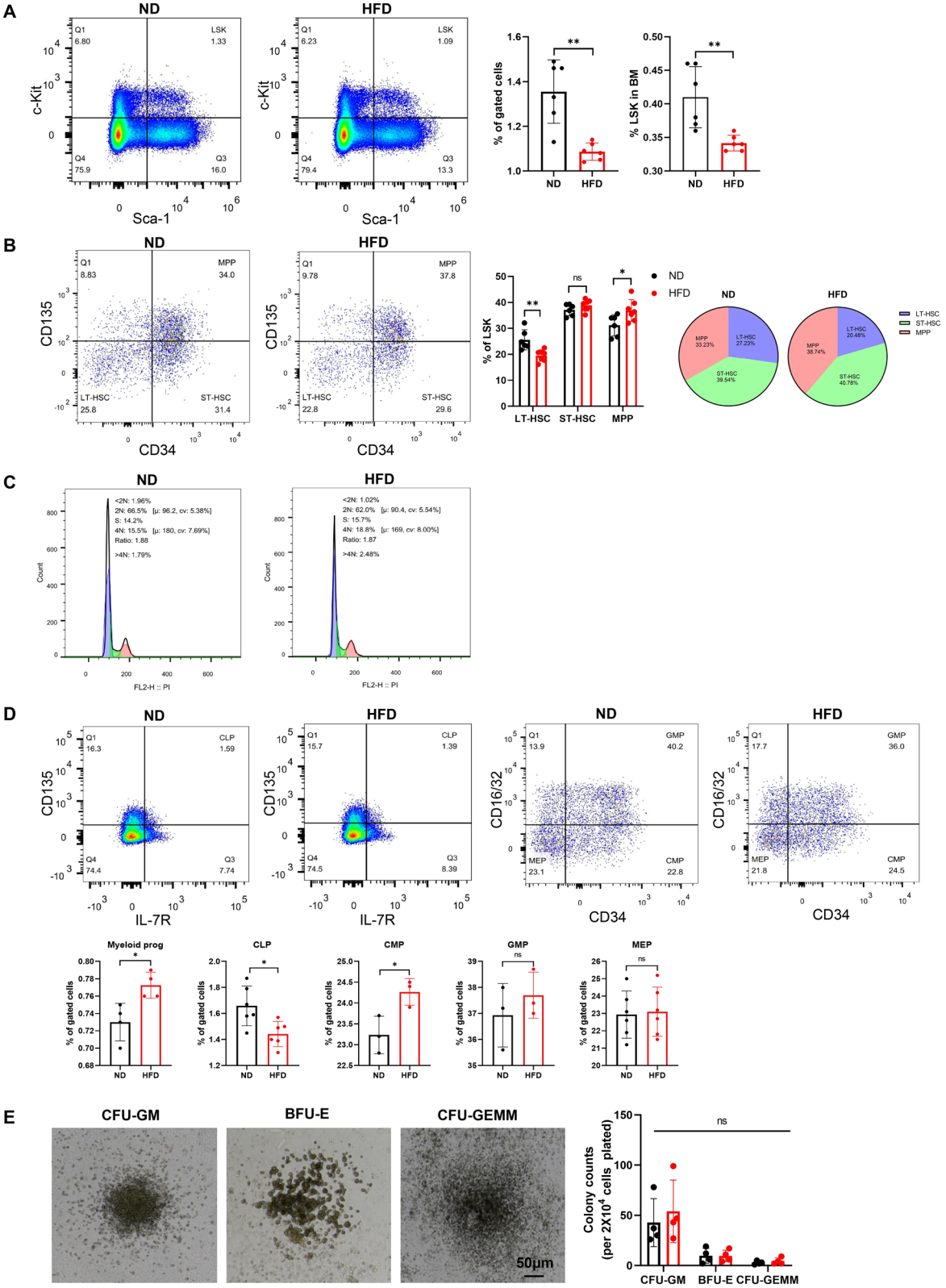


**Fig. 3** (See legend on previous page.)

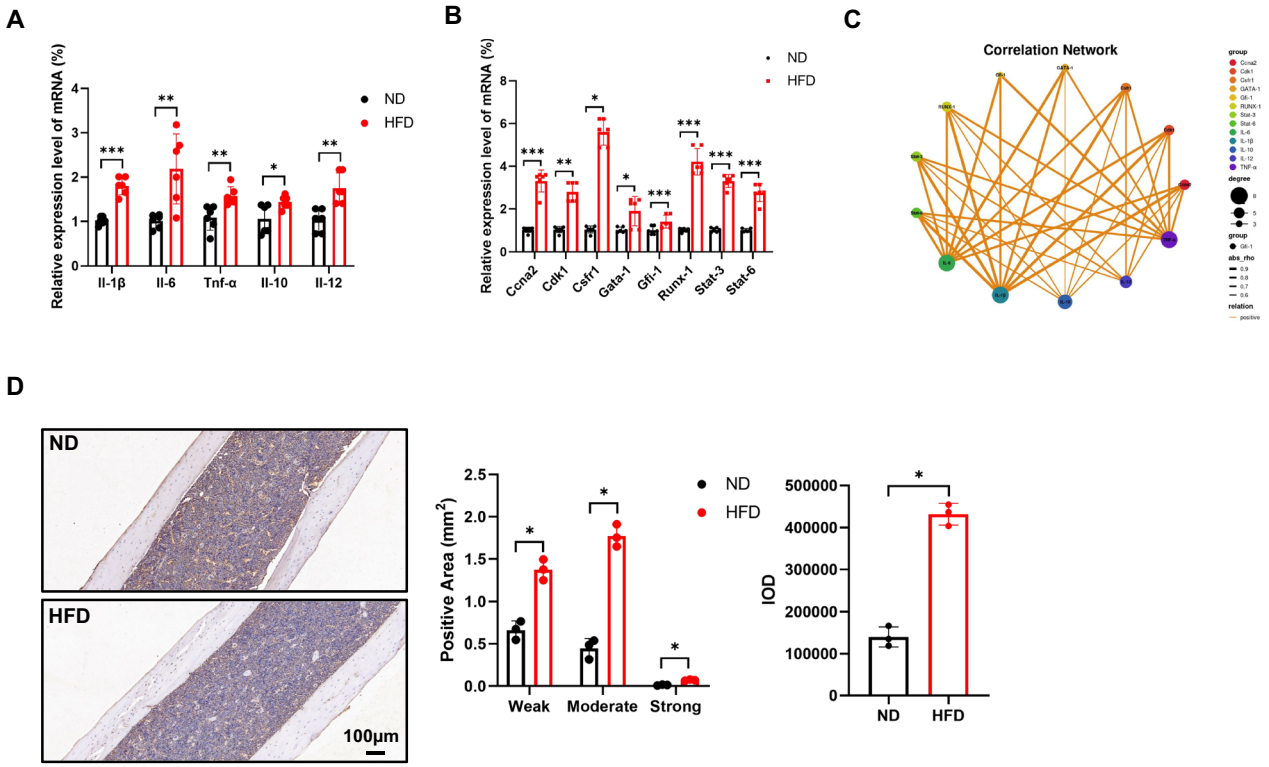


**Fig. 4** IL-1β is a critical factor that triggers changes in HSCs. (**A**) Expression level of inflammatory genes in bone marrow niche; (**B**) Expression level of HSCs function gene; (**C**) Correlation network and heat map. (**D**) Bone marrow immunohistochemistry of IL-1β. (data = mean ± standard error, * represents a significant difference compared with ND group, *$p < 0.05$, **$p < 0.01$, ***$p < 0.001$, ****$p < 0.0001$, ns represents no significant difference between the two groups)

response", "cell differentiation", "immune response", "positive regulation of population proliferation", and other biological processes, with a higher number of significantly upregulated genes (Fig. 5C). Results from the KEGG pathway enrichment analysis indicated that these significantly upregulated genes were enriched in multiple pathways, such as "osteoclast differentiation", "leukocyte transendothelial migration", "hematopoietic cell lineage", and the "IL-17 signaling pathway" (Fig. 5D). Notably, the MAPK signaling pathway emerged as a central component within these key pathways. Intriguingly, IL-1β was identified as an inflammatory signal for the activation of the p38/MAPK signaling pathway. Furthermore, the transcriptome data revealed that the expression of *Il-1β* between the HFD and ND groups was equivalent, indicating that LK cells make no contribution to the increase of IL-1β in the obesity-associated bone marrow microenvironment (Fig. 5E). Subsequently, based on the screening results of the transcriptome data, the expression of genes within the p38/MAPK pathway was further assessed, revealing significant overexpression of several pivotal genes involved in this pathway, including *Il-1r1*, *Myd88*, *Irak4*, *Mapk13*, and *MK2* (Fig. 5F). *Il-1r1* has been recognized as which is interact with IL-1β to active the p38/MAPK pathway [27]. The IL-1β-mediated p38/MAPK signaling pathway provides a new perspective on the mechanism underlying obesity-induced changes in HSC fate decision.

(See figure on next page.)

**Fig. 5** HFD causes changes in the transcriptome of hematopoietic stem progenitor cells. (**A**) Pearson correlation and PCA; (**B**) Volcano plot of differential genes; (**C**) Histogram of the number of genes enriched by GO and the p value of TOP20 biological process term; (**D**) Histogram of the number of genes enriched by KEGG and KEGG pathway of p value TOP20; (**E**) The FPKM value of *Il-1β* in the sequenced cells; (**F**) Expression level of genes in p38/MAPK pathway. (A ~ D n = 3, data = mean ± standard error, * represents a significant difference compared with ND group, *$p < 0.05$, **$p < 0.01$, ***$p < 0.001$, ****$p < 0.0001$, ns represents no significant difference between the two groups)

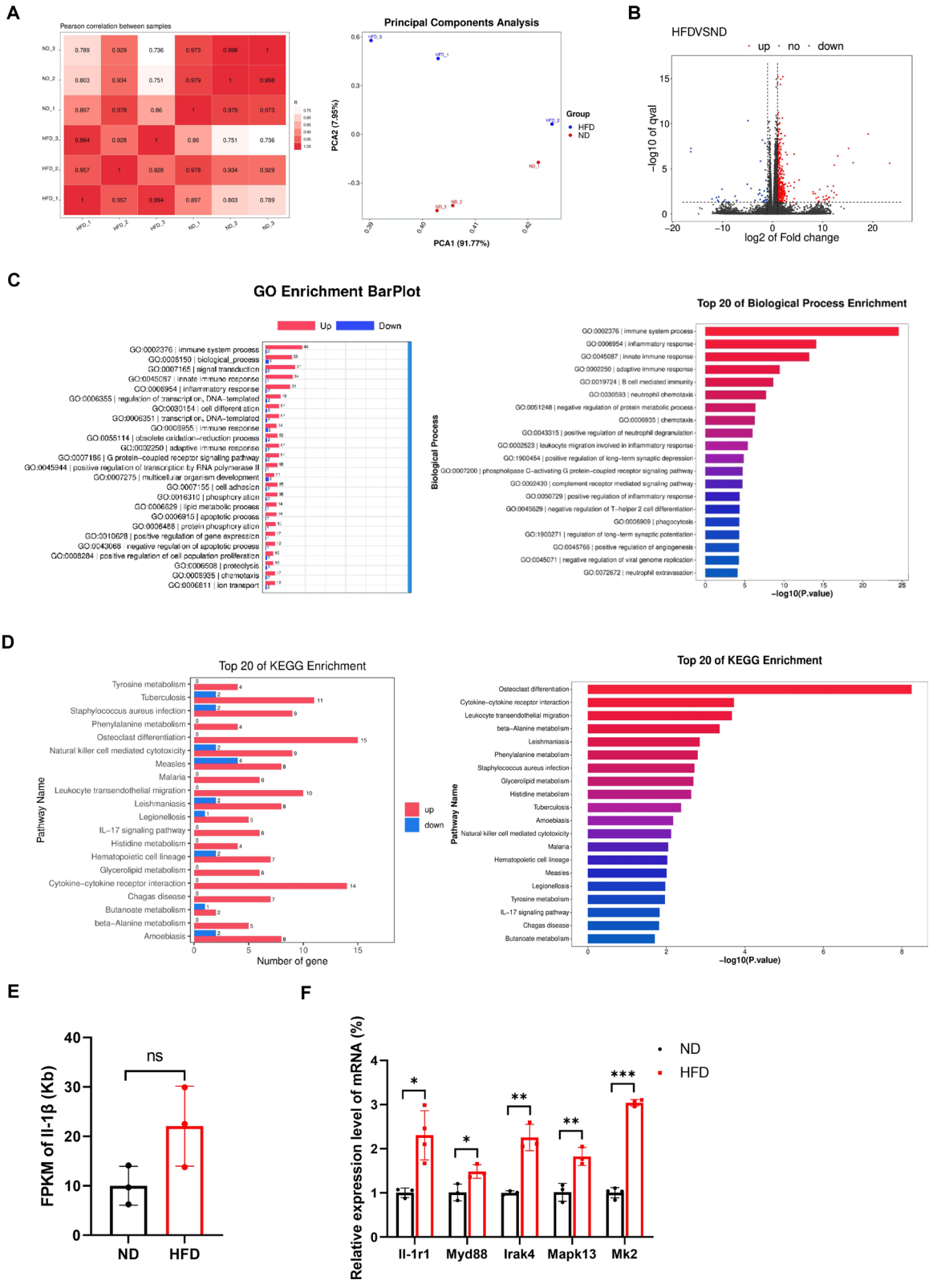


**Fig. 5** (See legend on previous page.)

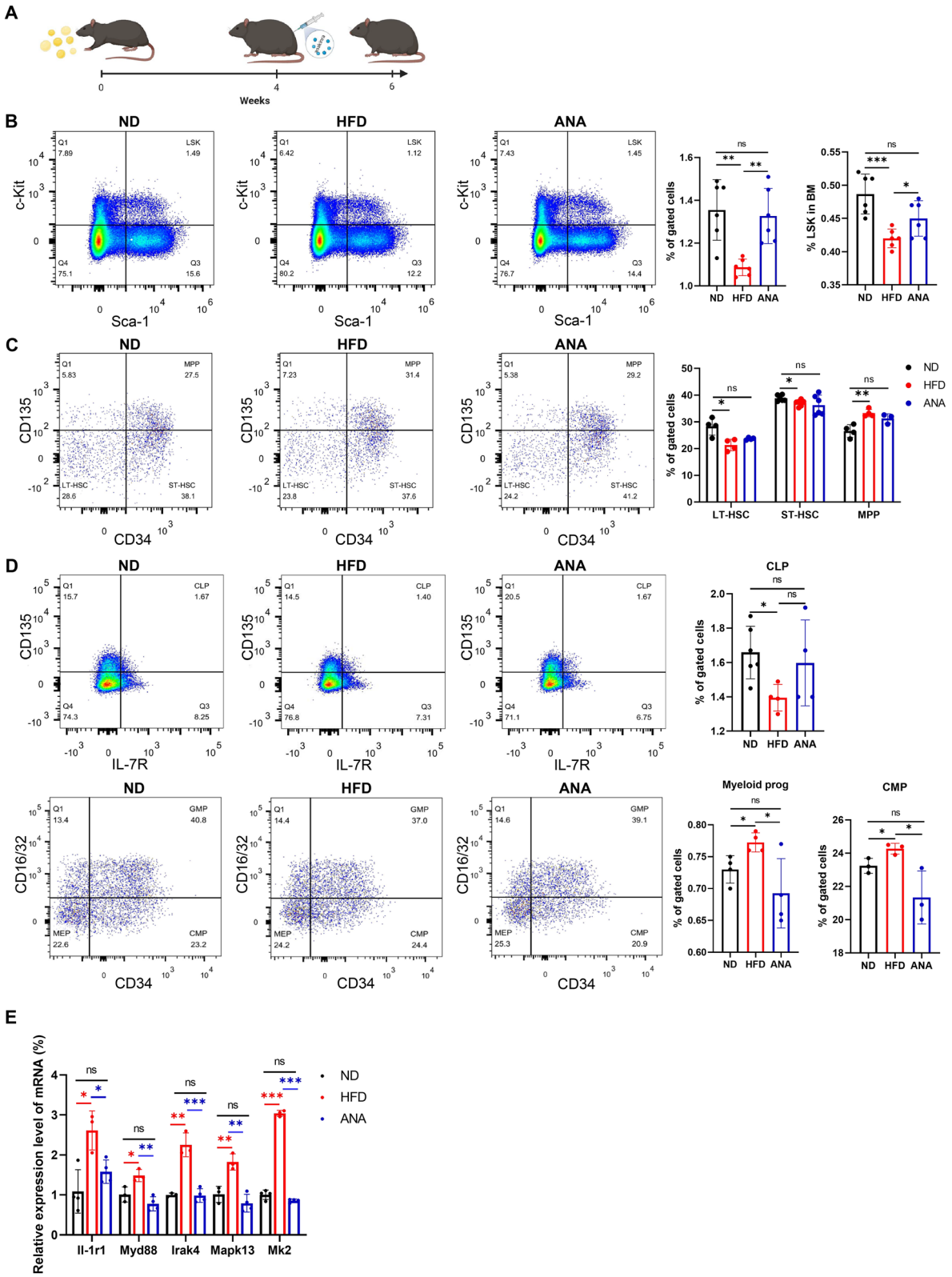


**Fig. 6** Inhibition of IL-1β Changes in parameters caused by obesity. (**A**) Experimental scheme; (**B**) Statistics of the proportion of LSK cells in bone marrow mononuclear cells; (**C**) Proportion of LSK cell subsets; (**D**) Lineage differentiation of hematopoietic stem progenitor cells; (**E**) Expression level of genes in p38/MAPK pathway after anakinra treatment. (data = mean ± standard error, * represents a significant difference compared with ND group, *$p < 0.05$, **$p < 0.01$, ***$p < 0.001$, ****$p < 0.0001$, ns represents no significant difference between the two groups)

### Rescue obesity-induced HSC fate changes through IL-1β inhibition: a promising outcome

To investigate whether the effects of HFD on HSCs could be counteracted by interfering with the interaction of IL-1β and IL-1r1 and reducing the activation of p38/MAPK signaling, the human IL-1β receptor antagonist anakinra was administered for a duration of 14 days during the development of obesity in mice [28] (Fig. 6A). After 6 weeks of HFD, the proportion of LSK cells within the bone marrow was analyzed. The results demonstrated that mice treated with anakinra exhibited an increased percentage of LSK cells (Fig. 6B), and the proportions of HSC subpopulations, including LT-HSCs, ST-HSCs and MPPs (Fig. 6C). In addition, the differentiation patterns of myeloid and lymphoid lineages in the anakinra-treated bone marrow showed the same tend as that observed in the ND group (Fig. 6D). Furthermore, gene expression analysis indicated that key genes within the p38/MAPK signaling pathway were significantly downregulated following anakinra treatment, similar to the levels observed in the ND group (Fig. 6E). Collectively, these findings suggest that short-term blockade of IL-1β-induced p38/MAPK signaling has the potential to ameliorate the HFD-induced HSC fate transition.

## Discussion

Herein we demonstrate that exposure to a HFD reduces the pool of HSCs and promotes the differentiation of HSCs toward myeloid lineages. Previous studies have indicated that obesity can lead to diverse alterations in the HSC pool, including both its expansion in some cases [29, 30] and contraction in others [16, 31]. These studies have also revealed that HFD significantly reduced the proportion of LT-HSCs and increased the proportion of MPPs [17]. HSC in the HFD mice bone marrow exhibited an actively differentiating towards myeloid lineages, in accordance with Cho's study [32]. Lou et al. [17] reveal that HFD alters the HSC niche by increasing bone marrow adiposity via activation of PPARγ2, which can be recapitulated via microbiota transfer from obese mice. Lee et al. [16] demonstrate that obesity produces durable in HSC function and the oxidative environment is a key driver. However, previous studies on the impact of inflammation on bone marrow HSCs were not based on obesity, and the research on the inflammation-mediated changes in HSC fate during the process of obesity has many gaps.

Inflammation is a hallmark of obesity [33]. Various inflammatory cytokines have been confirmed to affect HSCs in different ways, such as TNF-α [34], TGF-β [35], and IFN-γ [36] [37]. Studies also have revealed that chronic IL-1β exposure drives HSCs towards precocious myeloid differentiation at the expense of self-renewal [38]. We initially hypothesize that obesity creates an inflammatory environment within the HSC niche, which act as a regulator for HSC fate decision and strongly correlates with alterations in HSC differentiation [39–41]. After a systematic analysis of changes in the physicochemical properties of the bone marrow, we demonstrated the high expression of inflammatory cytokines, including significantly elevated IL-1β by HFD and revealed a close relevance between obesity-promoting IL-1β with the molecular changes in bone marrow HSCs. Inhibition of IL-1β restored the number of HSCs and rescued the dysregulated HSC differentiated fate in bone marrow, highlighting the distinctive role of IL-1β in driving HSC activation during obesity development. Li et al. used a periodontitis-induced trained phenotype to show that IL-1β signaling in HSCs is essential for the sustained enhancement of myelopoiesis [42]. Transcriptomic profiling revealed the activation of the p38/MAPK signaling pathway in HSCs following HFD exposure. The higher expression of *IL-1r1* further indicated that IL-1β emerged as a potential activator of this pathway. Blocking IL-1β-induced signaling attenuated HSC activation, elevated HSCs proportions, and mitigated the myeloid differentiation biases, which is accordance with the results from Li et al. [42]. These findings provide novel insights into the mechanisms of IL-1β as a candidate target for the prevention of inflammatory-induced HSC fate alterations.

From a clinical standpoint, these results offer a novel perspective for understanding the mechanism of bone marrow hematopoietic homeostasis in response to the obesity. It is worth mentioning that when assessing the physical properties of the HSC niche, a significant decrease in the Young's modulus of the bone marrow was found. The contribution of obesity-induced changes in tissue stiffness that could direct regulate the fate decision of HSCs, will be future clarified. Furthermore, additional first and second transplantation assays should be conducted to provide functional evidence that obesity indeed impacts HSC function. François et al. conducted a study to investigate the effects of HFD on the maintenance and functionality of HSCs [35]. Their findings revealed that, compared to controls, the total bone marrow cells harvested from mice fed with HFD demonstrated a notably reduced capacity for long-term reconstitution in both peripheral blood and bone marrow, as assessed 16 weeks post-transplantation. Furthermore, the researchers observed a shift in the reconstitution pattern of bone marrow cells sourced from HFD-fed mice. Specifically, these cells gave rise to a higher proportion of mature myeloid lineage cells in the peripheral blood, whereas the reconstitution of T-lymphocytes was significantly impaired, and the reconstitution of B-lymphocytes remained unaffected by the HFD exposure. This suggests

that HFD not only changes the fate of HSC, but also changes the function of HSC.

Numerous obesity-related maladies are intrinsically linked to hematopoietic system dysregulation, mirroring the intricate interplay between inflammation and obesity [43]. This bolsters the notion that microenvironmental inflammation profoundly impacts HSC fate transitions. Understanding the therapeutic potential of modulating the HSC microenvironment to ameliorate metabolic disorders in obesity represents a promising research direction. Future investigations may scrutinize the interplay of inflammation with hematopoiesis through the HSC niche. However, the potential contributions of other inflammatory cytokines remain enigmatic. Quantifying the individual impact of these factors on HSC fate modification remains a formidable challenge. Consequently, the pursuit of optimal anti-inflammatory strategies to reverse HSC fate changes induced by HFD and their potential to alleviate obesity-related metabolic dysregulation warrants further investigation. Moreover, it is imperative to delve into the root causes of obesity-induced inflammatory states. Unraveling the temporal and spatial sequences and causal links between inflammation, metabolic alterations, and disease onset poses an intriguing avenue for future exploration. It is top priority task to ascertain whether interventions targeting specific nutrients or metabolic pathways can mitigate obesity-associated inflammation, potentially reverting HSC fate changes. This necessitates comprehensive research to elucidate the intricate web of relationships among metabolism, inflammation, and HSC dynamics.

## Conclusions

Our study advances the comprehension of the interplay among obesity, inflammation, and hematopoiesis. It has been demonstrated that the p38/MAPK signaling pathway in HSCs is activated by elevated levels of IL-1β within the HSC niche in obese models, thereby regulating hematopoietic stem cell differentiation. Undeniably, further research is necessary to unravel the complexities of how inflammation affects the fate of HSCs and its far-reaching implications for obesity-related disorders.

### Abbreviations

| | |
|---|---|
| CLP | Common lymphoid progenitor |
| CMP | Common myeloid progenitor |
| FBS | Fetal bovine serum |
| GMP | Granulocyte/monocyte progenitor |
| GO | Gene ontology |
| HFD | High-fat diet |
| HSCs | Hematopoietic stem cells |
| KEGG | Kyoto Encyclopedia of Genes and Genomes |
| LSK | $Lin^-$, $Sca\text{-}1^+$, $c\text{-}Kit^-$ |
| LT-HSCs | Long-term HSCs |
| MEP | Megakaryocyte/erythrocyte progenitor |
| MPP | Multipotent progenitors |
| ND | Normal diet |
| PBS | Phosphate-buffered saline |
| SEM | Standard error of the mean |
| ST-HSCs | Short-term HSCs |

## Supplementary Information

The online version contains supplementary material available at https://doi.org/10.1186/s13287-024-03915-w.

Additional file 1.

### Acknowledgements

The authors acknowledge the all members of the Research Center of Special Environmental Biomechanics and Medical Engineering at Northwestern Polytechnical University. The authors express our gratitude to all the projects that have offered their support to facilitate this study. Furthermore, the authors declare that artificial intelligence is not used in this study.

### Author contributions

J.Y. and P.Z performed experiments and wrote the article. X.L. (Xiru Liu), C.P., G.S. and X.Z. (Xinmin Zheng) conducted the statistical analysis. X.L. (Xiang Li), P.Y. and X.Z. (Xiaohang Zou) reviewed the article and provided suggestions. H.Y. and Y.L. conceptualization, supervision, funding acquisition, writing-review, and editing. All authors have read and agreed to the published version of the manuscript.

### Funding

Project supported by Nanjing medical science and technology development fund, ZKX21014.

### Availability of data and materials

All data relevant to the study are included in the article or uploaded as online supplemental information.

## Declarations

### Ethics approval and consent to participate

The ethics approval for the research project titled "Effect of obesity induced by high-fat diet on proliferation and differentiation of hematopoietic stem cells and its mechanism" was granted by the Medical and Laboratory Animal Ethics Committee of Northwestern Polytechnical University. The approval number for this project is 202301168, and the date of approval is 1/3/2023. All animals involved in the study were handled in accordance with ethical guidelines, and their care and use were approved by the Medical and Laboratory Animal Ethics Committee of Northwestern Polytechnical University.

### Consent for publication

Not applicable.

### Competing interests

The authors declare no competing interests.

### Author details

[1]School of Life Sciences, Northwestern Polytechnical University, Xi'an, Shaanxi, China. [2]Engineering Research Center of Chinese Ministry of Education for Biological Diagnosis, Treatment and Protection Technology and Equipment, Xi'an, Shaanxi, China. [3]Center of Special Environmental Biomechanics and Biomedical Engineering, Northwestern Polytechnical University, Xi'an, Shaanxi, China. [4]School College of Food Science and Engineering, Shaanxi University of Science & Technology, Xi'an, Shaanxi, China. [5]Department of Mechanical Engineering, University of Victoria, Victoria, BC, Canada. [6]Department of Cardiology, Nanjing University Medical School Afliated Nanjing Drum Tower Hospital, Nanjing, Jiangsu, China.

Received: 3 May 2024 Accepted: 30 August 2024
Published online: 29 September 2024

**References**

1. Bluher M. Obesity: global epidemiology and pathogenesis. Nat Rev Endocrinol. 2019;15(5):288–98.
2. Liu X, Yang J, Yan Y, Li Q, Huang R-L. Unleashing the potential of adipose organoids: A revolutionary approach to combat obesity-related metabolic diseases. Theranostics. 2024;14(5):2075–98.
3. Rohm TV, Meier DT, Olefsky JM, Donath MY. Inflammation in obesity, diabetes, and related disorders. Immunity. 2022;55(1):31–55.
4. Bowers E, Singer K. Obesity-induced inflammation: the impact of the hematopoietic stem cell niche. JCI Insight. 2021. https://doi.org/10.1172/jci.insight.145295.
5. Wu H, Ballantyne CM. Metabolic inflammation and insulin resistance in obesity. Circ Res. 2020;126(11):1549–64.
6. Anttila V, Stefansson H, Kallela M, Todt U, Terwindt GM, Calafato MS, et al. Genome-wide association study of migraine implicates a common susceptibility variant on 8q22.1. Nat Genet. 2010;42(10):869–73.
7. Benova A, Tencerova M. Obesity-induced changes in bone marrow homeostasis. Front Endocrinol. 2020;11:294.
8. Van den Berg SM, Seijkens TT, Kusters PJ, Beckers L, den Toom M, Smeets E, et al. Diet-induced obesity in mice diminishes hematopoietic stem and progenitor cells in the bone marrow. FASEB J. 2016;30(5):1779–88.
9. Cortez M, Carmo LS, Rogero MM, Borelli P, Fock RAJI. A high-fat diet increases IL-1, IL-6, and TNF-α production by increasing NF-κB and attenuating PPAR-γ expression in bone marrow mesenchymal stem cells. Inflammation. 2013;36:379–86.
10. Zhang P, Zhang C, Li J, Han J, Liu X, Yang H. The physical microenvironment of hematopoietic stem cells and its emerging roles in engineering applications. Stem Cell Res Ther. 2019;10(1):327.
11. Li Z, He XC, Li L. Hematopoietic stem cells: self-renewal and expansion. Curr Opin Hematol. 2019;26(4):258–65.
12. Lee-Thedieck C, Spatz JP. Biophysical regulation of hematopoietic stem cells. Biomater Sci. 2014;2(11):1548–61.
13. Shi G, Zhang P, Zhang X, Li J, Zheng X, Yan J, et al. The spatiotemporal heterogeneity of the biophysical microenvironment during hematopoietic stem cell development: from embryo to adult. Stem Cell Res Ther. 2023;14(1):251.
14. Dzierzak E, Bigas AJCSC. Blood development: hematopoietic stem cell dependence and independence. Cell Stem Cell. 2018;22(5):639–51.
15. Hurwitz SN, Jung SK, Kurre PJL. Hematopoietic stem and progenitor cell signaling in the niche. Leukemia. 2020;34(12):3136–48.
16. Lee JM, Govindarajah V, Goddard B, Hinge A, Muench DE, Filippi MD, et al. Obesity alters the long-term fitness of the hematopoietic stem cell compartment through modulation of Gfi1 expression. J Exp Med. 2018;215(2):627–44.
17. Luo Y, Chen GL, Hannemann N, Ipseiz N, Kronke G, Bauerle T, et al. Microbiota from obese mice regulate hematopoietic stem cell differentiation by altering the bone niche. Cell Metab. 2015;22(5):886–94.
18. Mitchell CA, Verovskaya EV, Calero-Nieto FJ, Olson OC, Swann JW, Wang X, et al. Stromal niche inflammation mediated by IL-1 signalling is a targetable driver of haematopoietic ageing. Nat Cell Biol. 2023;25(1):30–41.
19. Liu X, Zhang H, Yan J, Li X, Li J, Hu J, et al. Deciphering the efficacy and mechanism of *Astragalus membranaceus* on high altitude polycythemia by integrating network pharmacology and in vivo experiments. Nutrients. 2022;14(23):4968.
20. Zhang X, Cao D, Xu L, Xu Y, Gao Z, Pan Y, et al. Harnessing matrix stiffness to engineer a bone marrow niche for hematopoietic stem cell rejuvenation. Cell Stem Cell. 2023;30(4):378–95.
21. Liu K-F, Niu C-S, Tsai J-C, Yang C-L, Peng W-H, Niu H-S. Comparison of area under the curve in various models of diabetic rats receiving chronic medication. Arch Med Sci. 2020. https://doi.org/10.5114/aoms.2019.91471.
22. Fathi E, Azarbad S, Farahzadi R, Javanmardi S, Vietor I. Effect of rat bone marrow derived-mesenchymal stem cells on granulocyte differentiation of mononuclear cells as preclinical agent in cellbased therapy. Curr Gene Ther. 2022;22(2):152–61.
23. Dai L, Yao M, Fu Z, Li X, Zheng X, Meng S, et al. Multifunctional metal-organic framework-based nanoreactor for starvation/oxidation improved indoleamine 2,3-dioxygenase-blockade tumor immunotherapy. Nat Commun. 2022. https://doi.org/10.1038/s41467-022-30436-y.
24. Zhang P, Xu L, Gao J, Xu G, Song Y, Li G, et al. 3D collagen matrices modulate the transcriptional trajectory of bone marrow hematopoietic progenitors into macrophage lineage commitment. Bioactive Mater. 2022;10:255–68.
25. Rafat A, Dizaji Asl K, Mazloumi Z, Movassaghpour AA, Talebi M, Shanehbandi D, et al. Telomerase inhibition on acute myeloid leukemia stem cell induced apoptosis with both intrinsic and extrinsic pathways. Life Sci. 2022;295:120402.
26. Wang JD, Chen WY, Li JR, Lin SY, Wang YY, Wu CC, et al. Aspirin mitigated tumor growth in obese mice involving metabolic inhibition. Cells. 2020;9(3):569.
27. Carey A, Cleary MM, Edwards DK, Eide CA, Traer E, McWeeney SK, et al. The pro-inflammatory cytokine interleukin-1 Is essential for clonal expansion and disease progression in acute myeloid leukemia. Blood. 2015;126(23):866.
28. De Boer B, Sheveleva S, Apelt K, Vellenga E, Mulder AB, Huls G, et al. The IL1-IL1RAP axis plays an important role in the inflammatory leukemic niche that favors acute myeloid leukemia proliferation over normal hematopoiesis. Haematologica. 2020;106(12):3067–78.
29. Nagareddy PR, Kraakman M, Masters SL, Stirzaker RA, Gorman DJ, Grant RW, et al. Adipose tissue macrophages promote myelopoiesis and monocytosis in obesity. Cell Metab. 2014;19(5):821–35.
30. Singer K, DelProposto J, Morris DL, Zamarron B, Mergian T, Maley N, et al. Diet-induced obesity promotes myelopoiesis in hematopoietic stem cells. Mol Metab. 2014;3(6):664–75.
31. Liu A, Chen M, Kumar R, Stefanovic-Racic M, O'Doherty RM, Ding Y, et al. Bone marrow lympho-myeloid malfunction in obesity requires precursor cell-autonomous TLR4. Nat Commun. 2018;9(1):708.
32. Cho K, Ushiki T, Ishiguro H, Tamura S, Araki M, Suwabe T, et al. Altered microbiota by a high-fat diet accelerates lethal myeloid hematopoiesis associated with systemic SOCS3 deficiency. iScience. 2021;24(10):103117.
33. Hsieh CC, Chiu HH, Wang CH, Kuo CH. Aspirin modifies inflammatory mediators and metabolomic profiles and contributes to the suppression of obesity-associated breast cancer cell growth. Int J Mol Sci. 2020;21(13):4652.
34. Pronk CJ, Veiby OP, Bryder D, Jacobsen SE. Tumor necrosis factor restricts hematopoietic stem cell activity in mice: involvement of two distinct receptors. J Exp Med. 2011;208(8):1563–70.
35. Hermetet F, Buffiere A, Aznague A, Pais de Barros JP, Bastie JN, Delva L, et al. High-fat diet disturbs lipid raft/TGF-beta signaling-mediated maintenance of hematopoietic stem cells in mouse bone marrow. Nat Commun. 2019;10(1):523.
36. Baldridge MT, King KY, Boles NC, Weksberg DC, Goodell MAJN. Quiescent haematopoietic stem cells are activated by IFN-γ in response to chronic infection. Nature. 2010;465(7299):793–7.
37. de Laval B, Maurizio J, Kandalla PK, Brisou G, Simonnet L, Huber C, et al. C/EBPbeta-dependent epigenetic memory induces trained immunity in hematopoietic stem cells. Cell Stem Cell. 2020;26(5):657–74.
38. Pietras EM, Mirantes-Barbeito C, Fong S, Loeffler D, Kovtonyuk LV, Zhang S, et al. Chronic interleukin-1 exposure drives haematopoietic stem cells towards precocious myeloid differentiation at the expense of self-renewal. Nat Cell Biol. 2016;18(6):607–18.
39. Geiger SS, Essers MAG. Inflammation's epigenetic footprint in hematopoietic stem cells. Cell Stem Cell. 2020;26(5):611–2.
40. King KY, Goodell MA. Inflammatory modulation of HSCs: viewing the HSC as a foundation for the immune response. Nat Rev Immunol. 2011;11(10):685–92.
41. Pietras EM. Inflammation: a key regulator of hematopoietic stem cell fate in health and disease. Blood. 2017;130(15):1693–8.
42. Li X, Wang H, Yu X, Saha G, Kalafati L, Ioannidis C, et al. Maladaptive innate immune training of myelopoiesis links inflammatory comorbidities. Cell. 2022;185(10):1709-27.e18.
43. Deng T, Lyon CJ, Bergin S, Caligiuri MA, Hsueh WA. Obesity, inflammation, and cancer. Mech Dis. 2016;11:421–49.

## Publisher's Note